Seeded-growth Aqueous Synthesis of Colloidal-Stable Citrate-Stabilized Au/CeO2 Hybrid Nanocrystals: Heterodimers, Core@Shell, Clover- and Star-like Structures.

Journal:	*Chemistry of Materials*
Manuscript ID	cm-2019-02005z.R2
Manuscript Type:	Article
Date Submitted by the Author:	26-Aug-2019
Complete List of Authors:	Piella, Jordi; Institut Català de Nanociència i Nanotecnologia, Gonzalez-Febles, Ana; Institut Català de Nanociència i Nanotecnologia Patarroyo, Javier; Institut Català de Nanociència i Nanotecnologia, Arbiol, Jordi; ICREA and Catalan Institute of Nanoscience and Nanotechnology (ICN2), CSIC and The Barcelona Institute of Science and Technology (BIST), Advanced Electron Nanoscopy Bastús, Neus; Institut Català de Nanociència i Nanotecnologia, Puntes, Víctor; Institut Catala de Nanotecnologia, Inorganic Nanoparticles Group

Seeded-growth Aqueous Synthesis of Colloidal-Stable Citrate-Stabilized Au/CeO_2 Hybrid Nanocrystals: Heterodimers, Core@Shell, Clover- and Star-like Structures.

Jordi Piella[1], Ana Gónzalez-Febles[1], Javier Patarroyo[1], Jordi Arbiol[1, 2], Neus G. Bastús[1]*, and Víctor Puntes[1, 2, 3]*

[1] Catalan Institute of Nanoscience and Nanotechnology (ICN2), CSIC & BIST, Campus UAB, Bellaterra, Barcelona, Spain.

[2] ICREA, Pg. Lluís Companys 23, 08010 Barcelona, Catalonia, Spain

[3] Vall d'Hebron Institut de Recerca (VHIR), 08035, Barcelona, Spain.

* To whom correspondence should be addressed: neus.bastus@icn2.cat, victor.puntes@icn2.cat

ABSTRACT

Well-defined colloidal-stable citrate-stabilized Au/CeO_2 hybrid nanocrystals (NCs) with coherent quasi-epitaxial interfaces and unprecedented control of their architectural and morphological characteristics have been synthesized via a novel and straightforward seeded-growth aqueous approach. The synthetic strategy, based on the identification of the experimental conditions under which the heterogeneous nucleation and growth processes of CeO_2 onto pre-synthesized Au is controlled, allows for the fine adjustment of each individual domain in the structure, particularly, the size of the Au core (from 5 to 100 nm), the thickness of the CeO_2 shell (from 5 to 20 nm) and the growth mode of CeO_2 onto Au NCs (from core@shell to heterodimer, clover- and star-like structures). This morphological control is achieved by the rational use of sodium citrate which plays multiple key roles, as a reducer and stabilizing agent in the preparation of the Au NCs, and as a complexing agent of Ce^{3+} for its controlled oxidation and hydrolysis during the subsequent CeO_2 deposition. The resultant Au/CeO_2 NCs remain stable and well-dispersed in water, allowing to study the impact of fine variations of NC structure on the underlying optical response. This level of morphological control, as well as the ease by which such well-defined nanostructures are produced, opens new opportunities for systematically investigate the interactions between individual components in designing more advanced complex NCs. Remarkably, because no organic solvents are used and no toxic waste is formed during the reaction, the proposed synthesis method can be defined as a sustainable, viable and low-cost effective.

INTRODUCTION

The rational design and development of new protocols for the colloidal synthesis of multicomponent nanocrystals (NCs) represent an important research direction to expand the functionalities of single-component counterparts.[1-3] In these systems, the functionality of the composite NCs is ultimately determined by the atomic interactions between constituent domains, which essentially relies on the precise and deliberate control of the NC architecture with the independent organization of each individual domain.[4] Thus, while in heterodimer conformation the accessible reactive sites at the interface enhance the catalytic performance of NCs[5-8], in core@shell geometries the interaction and electronic transfer between both domains are maximized, offering great applicability in plasmonics and sensing.[9-11]

Among the variety of developed materials, the controllable integration of noble metal and metal oxides into single NCs has attracted significant interest due to their unique structural features and physicochemical properties.[12-13] Despite advances in the field, the rational development of synthetic strategies enabling the precise control over the architecture of noble metal/metal oxide NCs and their interface still represents a difficult task, especially in water, where the identification of the relevant synthetic parameters governing their final morphology is a no solved issue. The deposition of a crystalline overlayer onto a crystalline substrate implies dealing with the atomic geometrical constraints of the materials involved, which is challenging for materials with large lattice mismatch. A paradigmatic case is Au/CeO_2 NCs. These materials are of interest because they have shown advanced optical properties and excellent catalytic activity due to the combination of the outstanding oxygen storage properties of CeO_2 facilitated by the metallic electron cloud of Au.[14-15]

Traditionally, Au/CeO_2 composites were easily prepared by impregnation and co-precipitation methods. The co-precipitation method takes advantage of the very low solubility of CeO_2 at alkaline pH, and because of its simplicity is the method of choice for industrial production, although the morphological control and stability of the resulting material is extremely poor.[16-18] Alternatively, colloidal chemistry strategies have allowed a much-improved control of material morphology.[19] Among them, one-pot methods based on the simultaneous oxidation and reduction of the precursors (Au^{3+} to Au^0 each 3 Ce^{3+} to Ce^{4+}), provide an easy way to force their precipitation into a single NC.[20-23] However, since Ce^{3+} oxidation and hydrolysis are promoted at alkaline pH and the reactivity of Au^{3+} in these conditions is very low[24], the redox process is not spontaneously favored, restricting the reaction conditions and thus hampering the architectural and morphological control of the system.

Alternatively, seed-mediated strategies have the advantage of decoupling Ce^{3+} oxidation from Au^{3+} reduction allowing to control these processes independently. However, the large lattice mismatch between CeO_2 (0.5412 nm) and Au (0.4065 nm), and the strong preference of cerium precursors to homonucleate during condensation rather than to heteronucleate makes the controlled deposition of CeO_2 at the surface of Au NCs difficult. In this regard, the complexation of Ce precursors with strong affinity ligands may provide a much lower hydrolysis rate which helps to avoid the homogeneous nucleation of CeO_2.[25]

Strategies exploiting the use of functional ligands to direct the deposition of CeO_2 onto pre-synthesized metal NCs are an interesting approach with increasing popularity.[25-28] Following this idea, ligands drive the absorption of Ce^{3+} and Ce^{4+} onto the metal surface that, upon heating, decomposes forming the hybrid structure. Stated examples include the use of EDTA,[25] CTAB,[25] glucose,[26] and mercaptocarboxilic acids.[27-28] Although interesting, these strategies are considerably complicated, often requiring multiple steps, including washing and functionalization of the pre-synthesized metal NCs, and post-thermal and –calcination treatments for the elimination of the ligands that may lead to unwanted NC transformations (sintering and aggregation).[21, 29-30] Additionally, the use of ligands with strong affinities for metal surface blocks further surface accessibility.

Herein, we report a general, straightforward and novel seeded-growth approach for the preparation of stable colloidal solutions of monodisperse citrate-stabilized Au/CeO_2 NCs with coherent and quasi-epitaxial interfaces. The method allows a fine adjustment of each individual domain in the structure and explicitly different coupling manners between the Au and CeO_2 counterparts. Particularly, the size of the Au core, the thickness of the CeO_2 shell and the growth mode of CeO_2 onto Au NCs can be manipulated in an independent, rational, and systematic way. The strategy relies on the use of sodium citrate (SC) as a unique co-reagent. SC is a well-known non-toxic and biocompatible substance widely-used in the synthesis of noble metal NCs.[31-32] In this work, we extend its use to oxide systems by employing its ability to act as a complexing agent of $Ce^{3+/4+}$ ions, thereby adjusting their oxidation and hydrolysis rates in water. Interestingly, because this strongly depends on the reaction pH, it is by adjusting this parameter that architectures varying from core@shell to clover-like and heterodimers can be obtained. In addition, Au can be overgrown onto clover-like Au@CeO_2 NCs, yielding to tip-free CeO_2-coated Au star-like NCs. Different morphologies entail different properties. Thus, while heterodimer morphologies offer accessibility to both domains, core@shell structures are more attractive when seeking electronic confinement.

The overall procedure is simple, highly reproducible and avoids time-consuming processes because it does not require calcination or any other complicated steps. Furthermore, resultant Au/CeO_2 NCs remain stable and well-dispersed in water, and show bright colors with well-defined surface plasmon resonances, allowing studying the impact of fine variations of hybrid nanostructure on the underlying optical response.

RESULTS and DISCUSSION

In order to control the nucleation and growth of CeO_2 exclusively onto previously synthesized Au NCs, our strategy is to provide a lower reactivity of Ce^{3+} precursor in water by its complexation with sodium citrate (SC).[25, 33] Thus, for the synthesis of core@shell Au@CeO_2 hybrid NCs, citrate-stabilized Au seeds of ~30 nm are first prepared as previously described[31] and used without further purification. The formation of the CeO_2 shell is achieved by injecting an aqueous solution of $Ce(NO_3)_3$ into a boiling solution of SC containing a specific amount of the Au seeds. The citrate rapidly complex and stabilize the Ce^{3+} ions that, upon boiling at alkaline conditions, slowly oxidize -by dissolved O_2-, hydrolyze and deposit at the metal surface, leading to Au@CeO_2 NCs. This process results in a progressive change in the color of the reaction mixture from red-wine (Au seeds) to bright/intense purple (Au@CeO_2 NCs), and takes about 4 hours to complete.

Representative images of transmission electron microscopy (TEM) and high-angle annular dark field scanning TEM (HAADF-STEM) of as-obtained colloids (**Fig. 1A-D)** show the systematic formation of highly monodisperse Au@CeO_2 NCs consisting of an electron-dense core of Au (~30 nm) surrounded by a relatively uniform crystalline CeO_2 shell (~7 nm). Interestingly, no isolated CeO_2 were observed in the final product, indicating the controlled growth of CeO_2 onto the Au NC surface. According to HRTEM images (**Fig. 1E, S1-2**), the shell is composed of tiny CeO_2 NCs with sizes between 2-3 nm, assembled together around the Au core with coherent quasi-epitaxial interfaces. Details of the squared region and its corresponding power spectrum reveal that the individual CeO_2 NCs are crystalline with lattice space corresponding well with the characteristic (111), (002) and (220) planes of fluorite phase of CeO_2. These results are further supported by the XRD analyses (**Fig. S3**). Finally, elemental chemical composition maps obtained by electron energy loss spectroscopy (EELS) (**Fig. 1F**) of selected Au@CeO_2 NCs (**Fig. 1D**) corroborate the encapsulation of the Au core by the CeO_2 NCs.

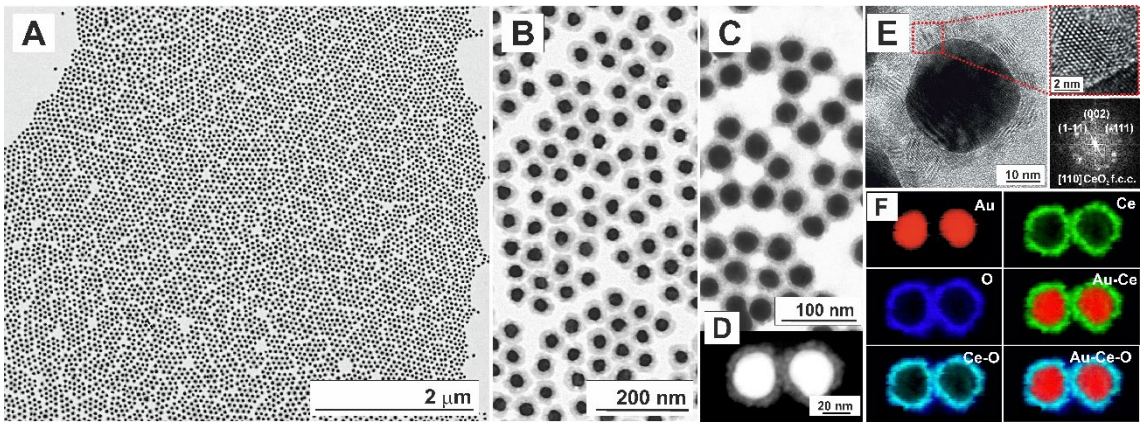

Figure 1. Synthesis of Au@CeO_2 Hybrid Nanocrystals. Representative TEM images (**A-C**) and HAADF-STEM images (**D**) of as-obtained Au@CeO_2 NCs revealing the formation of highly monodispersed hybrid nanostructures consisting on an electron-dense core of Au (~30 nm) surrounded by a relatively uniform crystalline CeO_2 shell (~7 nm). HRTEM images (**E**) reveal the details of the CeO_2 shell, which is composed of small NCs with sizes of 2-3 nm assembled together around the Au core. Detail of the red squared CeO_2 region and its corresponding electron diffraction pattern show the f.c.c structure of the CeO_2 phase. Electron energy loss spectroscopy (EELS) elemental maps (**F**) obtained from selected hybrid NCs (**D**) confirms the core@shell structure. Additional HRTEM characterization of these NCs is shown in Fig. S1.

One of the main advantages of adopting a seeded-growth approach is the possibility to precisely and independently tailor the Au core and the CeO_2 shell dimensions.[31, 34] Thus, well-defined core@shell Au@CeO_2 NCs with different core sizes were obtained by using Au NC seeds with diameters of 6.5, 10, 15, 30, 40 and 100 nm (**Fig. 2, Table 1**). The impact of the CeO_2 coating in the localized surface plasmon resonance (LSPR) of these Au@CeO_2 NCs was studied by UV-Vis spectroscopy. The presence of the CeO_2 coating results in both an increase in the LSPR peak intensity of the Au core and a systematic red-shift of its position. The great shift, as large as 86 nm in the case of 100 nm Au cores with a CeO_2 shell of 18 nm, along with the increased absorbance of the samples, are in agreement with the high refractive index of the CeO_2 coating layer.[20, 25] Remarkably, the full width at half-maximum (FWMH) of the plasmon band is well-maintained, proving not only that the morphology of the initial Au seeds is preserved after the CeO_2 coating but also that the samples remain well-dispersed in solution. These changes in the optical properties upon the formation of the CeO_2 shell also result in color changes of the samples: from brown-red to pink-red (small Au cores, **Fig. 2H**), from red to purple (medium Au cores, **Fig. 2J**) and finally from red to blue (large Au cores, **Fig. 2L**).

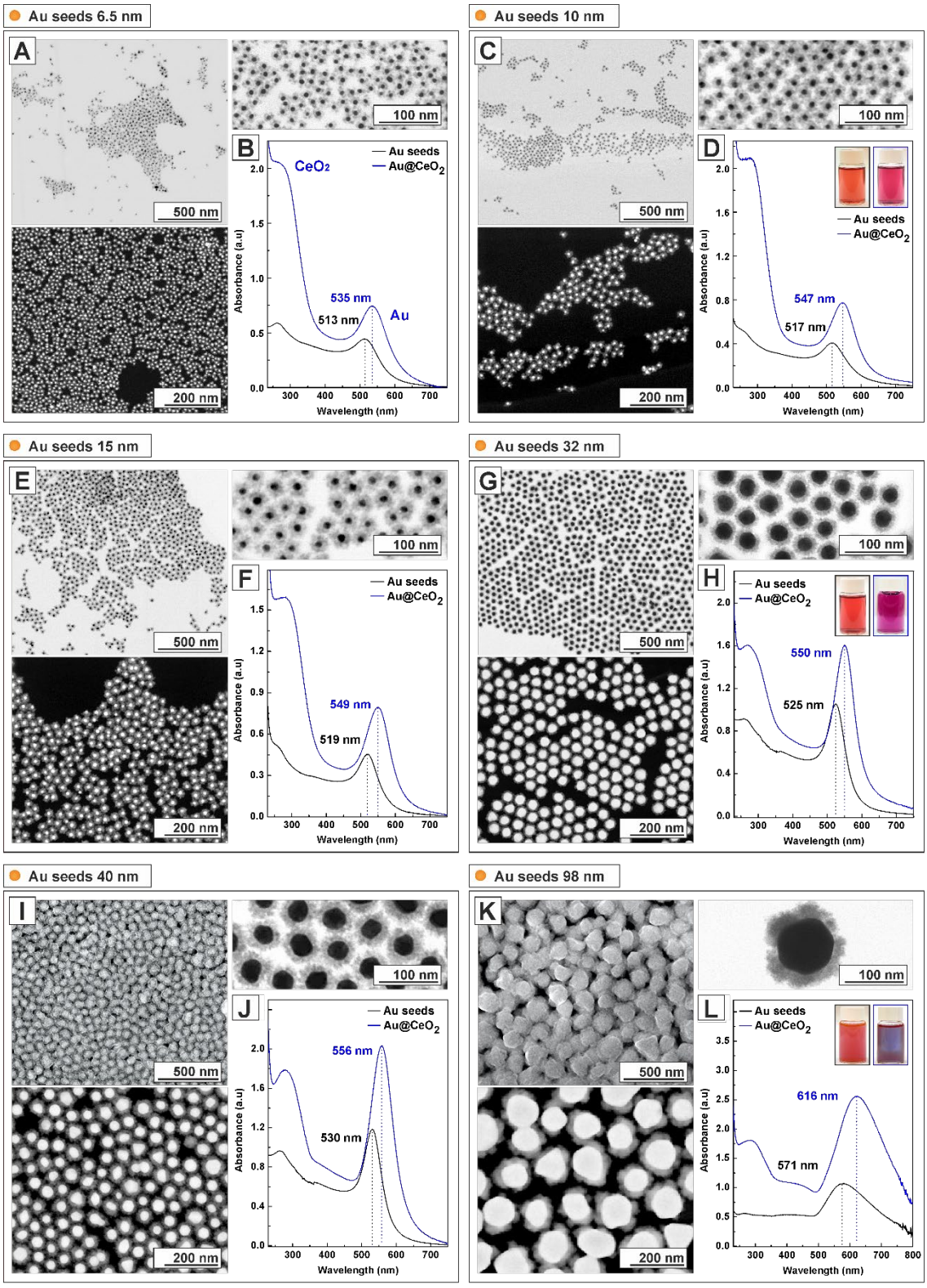

Figure 2. Size control of Au core in the synthesis of Au@CeO_2 Hybrid Nanocrystals. Representative TEM, SEM and HAADF-STEM images of well-defined core@shell Au@CeO_2 NCs with different core diameters, and corresponding UV–vis spectra before and after formation of the CeO_2 shell onto Au seeds of 6.5 nm (**A, B**), 10 nm (**C, D**), 15 nm (**E, F**), 32 nm (**G, H**), 40 nm (**I, J**) and 98 nm (**K, L**). In all cases, the LSPR peak of the initial Au seeds (black line) increases in intensity and red-shifts after the CeO_2 coating (blue line). Samples are detailed in **Table 1**.

Table 1. Tested conditions for the preparation of Au@CeO_2 NCs with controlled Au core size.

SAMPLE	SYNTHESIS CONDITIONS			TEM SIZE		LSPR POSITION		
	Au seeds diam. (nm)	[Au seeds] (NP/mL)*	$Ce(NO_3)_3$ (mL)**	Au core diam. (nm)	CeO_2 shell (nm)	Au λ (nm)	Au@CeO_2 λ (nm)	$\Delta\lambda$ (nm)
FIG.2A	6.5 ± 0.6	~1.1 10^{13}	1.5	6.8 ± 1.1	4.0 ± 0.7	513	535	22
FIG.2C	9.9 ± 0.8	~2.5 10^{12}	1.5	9.7 ± 1.5	6.6 ± 1.2	517	547	30
FIG.2E	14.6 ± 1.3	~7.8 10^{11}	1	14.8 ± 1.8	7.2 ± 1.2	519	549	30
FIG.2G	32.0 ± 2.6	~1.3 10^{11}	0.6	31.9 ± 2.6	6.6 ± 0.9	525	550	25
FIG.2I	40.1 ± 3.8	~6.8 10^{10}	0.6	40.3 ± 3.9	8.3 ± 0.9	530	560	26
FIG.2K	98.3 ± 16.0	~5.9 10^{9}	0.75	98.5 ± 15.6	18.4 ± 4.3	571	616	45

***100 mL of a citrate solution (5 mM) with adjusted pH 9-10. **Specific volume of a 25 mM solution.**

The method also allows the fine adjustment of the amount of CeO_2 deposited onto the Au cores by simply adjusting the ratio between Au seeds to Ce^{3+} precursor (**Fig. 3, Table 2**). Thus, the addition of low amounts of Ce^{3+}, or alternatively the increased number of seed NCs present in solution, leads to the formation of non-uniform clover-like structures with uncompleted shell morphologies (**Fig. 3A, D**) that become complete core@shell structures when the amount of Ce^{3+} was increased (**Fig. 3B-C, D-F**). As a result, clover-like Au@CeO_2 NCs, where parts of the Au surface are still exposed, experience smaller red-shifts than NCs with a uniform and thick CeO_2 coating around the Au cores (**Fig. 3G, H**).[35] A further increase of injected Ce^{3+}, required for the formation of thicker CeO_2 shells (>20 nm) in a single step, results in the nucleation of separate CeO_2 NCs. In this case, the sequential and slow injections of Ce^{3+} precursor prevents the system from self-nucleation,[31] thereby leading to the formation of thicker CeO_2 shells. Note that the possibility to adjust the thickness and dimensionality of the CeO_2 shell is important to design the final applicability of the NC. Thus, while the thinner and low compact shell in the clover-like structures maximize the exposed interface between both materials and provides a shorter diffusion pathway for reactants to reach the Au core, the thicker and uniform shell endows the NC with long-term stability against chemical transformations (dissolution and aggregation).[36]

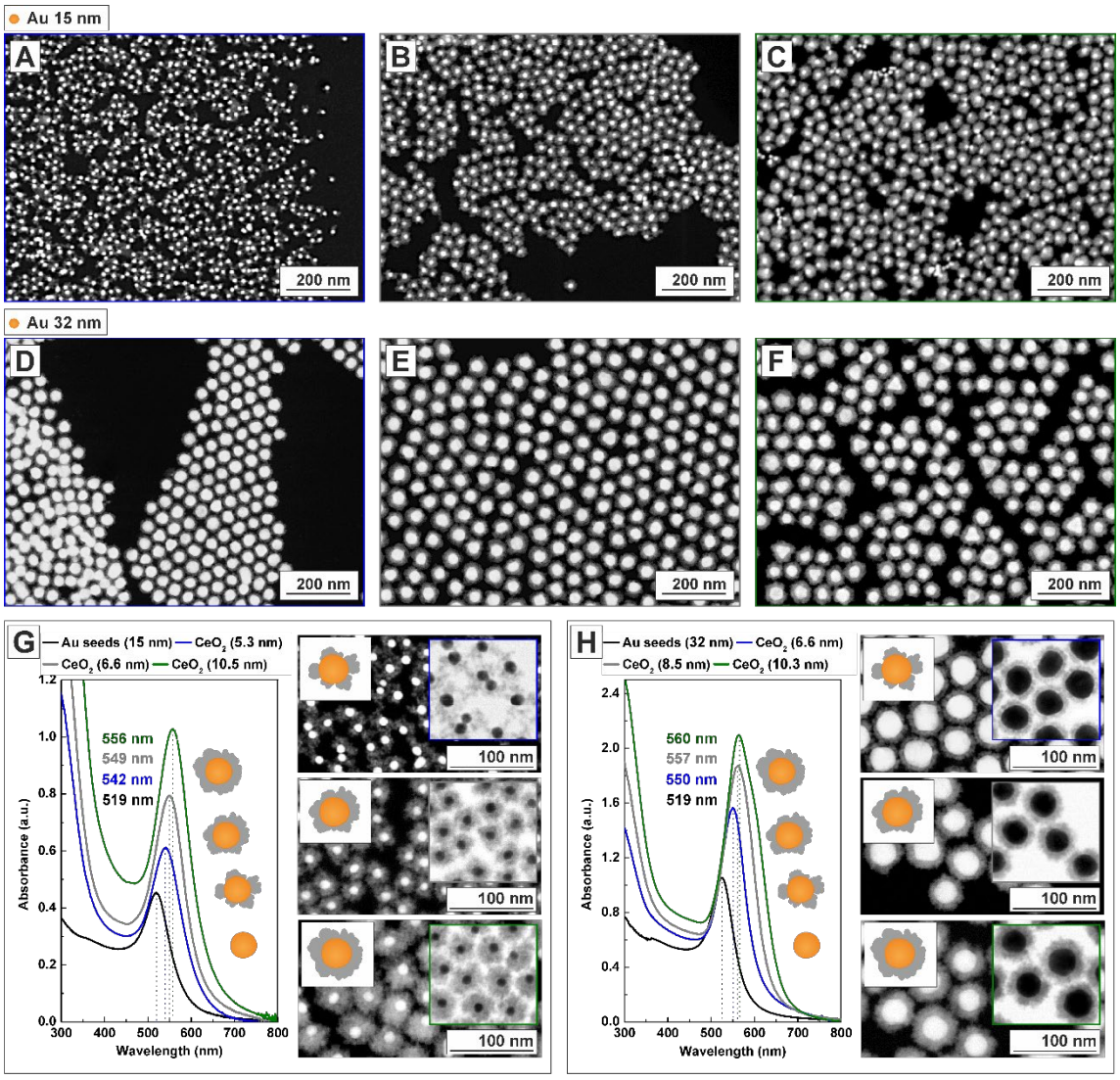

Figure 3. Control of CeO_2 shell thickness in the synthesis of Au@CeO_2 Hybrid NCs. Representative TEM and HAADF-STEM images of core@shell Au@CeO_2 NCs with increasing CeO_2 shell thickness (**A-F**): Au cores of 15 nm with increasing CeO_2 shell from 5.3 nm (**A**), 7.2 nm (**B**) and 10.5 nm (**C**), and Au cores of 32 nm with increasing CeO_2 shell from 6.6 (**D**), 8.5 (**E**) and 10.3 nm (**F**). UV-vis spectra of the corresponding Au colloids before and after CeO_2 shell formation (**G, H**) reveals a strong dependence between the LSPR peak (intensity and position) and the thickness of the CeO_2 shell. Synthesis conditions are detailed in **Table 2**.

Table 2. Tested conditions for the preparation of Au@CeO_2 NCs with controlled CeO_2 shell thickness.

SAMPLE	SYNTHESIS CONDITIONS			TEM SIZE		LSPR POSITION		
	Au seeds diam. (nm)	[Au seeds] (NP/mL)*	$Ce(NO_3)_3$ (mL)**	Au core diam. (nm)	CeO_2 shell (nm)	Au λ (nm)	Au@CeO_2 λ (nm)	Δλ (nm)
FIG.2A	14.6 ± 1.3	~7.8 10^{11}	0.75	14.8 ± 1.6	5.3 ± 1.1	519	542	23
FIG.2C	14.6 ± 1.3	~7.8 10^{11}	1	14.8 ± 1.8	7.2 ± 1.2	519	549	30
FIG.2E	14.6 ± 1.3	~7.8 10^{11}	2.5	15.7 ± 1.8	10.5 ± 1.8	519	556	37
FIG.2G	32.0 ± 2.6	~1.3 10^{11}	0.6	31.9 ± 2.6	6.6 ± 0.9	525	550	25
FIG.2I	32.0 ± 2.6	~1.3 10^{11}	1	32.1 ± 2.6	8.5 ± 0.9	525	557	32
FIG.2K	32.0 ± 2.6	~1.3 10^{11}	1.5	32.8 ± 2.9	10.3 ± 1.5	525	560	35

***100 mL of a citrate solution (5 mM) with adjusted pH 9-10. **Specific volume of a 25 mM solution.**

The controlled deposition of CeO_2 domains onto the surface of Au seeds is promoted by the use of SC, which plays multiple roles (**Scheme 1**). Note that citrate already acts as a reducer and stabilizer in the synthesis of the Au seeds, providing electrostatic repulsion to the resultant Au NCs (role#1 and #2).[31] Next, in the formation process of the CeO_2 shell, citrate efficiently complex $Ce^{3+/4+}$ leading to a precursor with a much lower oxidation and hydrolysis rates (role#3) (**see SI**).[33] In a control experiment (**Fig. S5**), the lack of SC led to the formation of isolated and strongly aggregated CeO_2 NCs, indicating how the greater stability of the citrate-complexed $Ce^{3+/4+}$ precursor favours the formation of Au@CeO_2 NCs. Also, the employed SC solution maintains the reaction mixture at mild alkaline conditions, thereby promoting the oxidation of Ce^{3+} to Ce^{4+} by the dissolved O_2 but not its precipitation in the form of $Ce(OH)_3$, a step often required in the formation of the CeO_2 shell (role#4).[29] Note that in the absence of oxygen (in deoxygenated water), neither oxidation of Ce^{3+} nor deposition of a $Ce(OH)_3$ shell were observed as control experiments show (**Fig. S6**). Finally, the well-known affinity of carboxylic groups of citrate for metal and metal oxide surfaces ensures the colloidal stability of the resultant Au@CeO_2 NCs[25, 27-28] (role#5), as zeta potential measurements reveal (**Fig. S7**). Remarkably, this interaction with citrate does not prevent further functionalization of the NCs with the molecules of interest (**Fig. S8**).

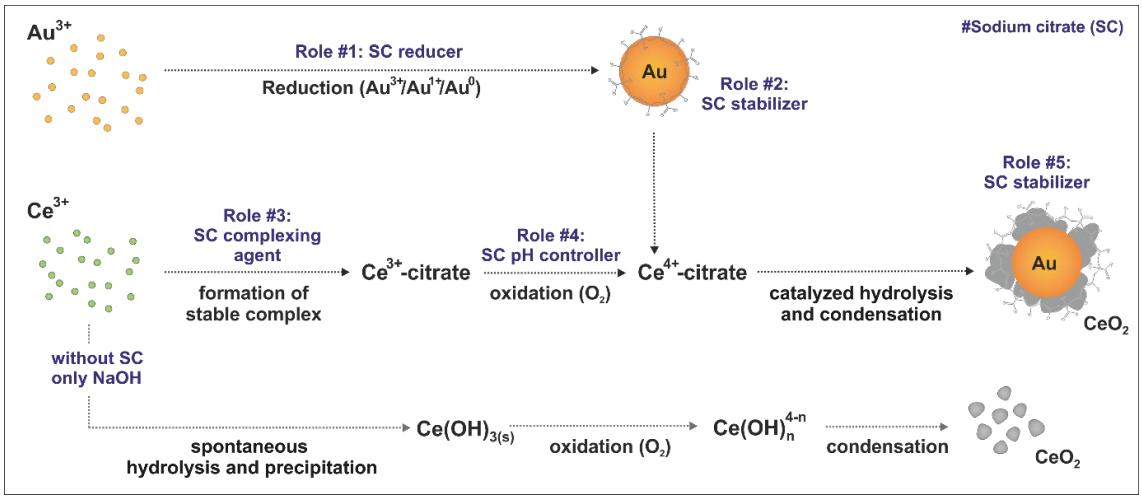

Scheme 1. Roles of SC in the Synthesis of Au@CeO_2 Hybrid NCs. Citrate acts as a reducer and stabilizer in the synthesis of Au seeds. Then, during the formation process of CeO_2, it effectively complex Ce^{3+} and Ce^{4+} ions, preventing their spontaneous hydrolysis and precipitation in water. The buffer effect of sodium citrate also prevents the solution pH from dropping towards acidic values during the synthesis and favours the oxidation of Ce^{3+} to Ce^{4+}. Finally, citrate adsorbs on the CeO_2 surface through their carboxylic groups and keeps the Au@CeO_2 NCs well-dispersed in solution.

Because the complexation of Ce^{3+} and Ce^{4+} with citrate forming intermediate species is expected to be strongly dependent on the pH, the effect of this parameter on the reaction kinetics and final NC structure was evaluated. By performing the reaction at acidic pH 5.5, partially substituting SC by citric acid, no deposition of CeO_2 onto the Au seeds was observed (**Fig. S9A**). Under these conditions, Ce^{3+} did not oxidize nor hydrolyze, even in the presence of a metal surface. When the pH was set at nearly neutral values (pH 7-8), the reaction proceeded very slow (5h) (**Fig. S10A**) and resultant NCs were heterodimers composed by two well-defined compositional domains (**Fig. 4A-B, S11**). As pH was increased (pH 9-10), the reaction progressed faster (1-2h) (**Fig. S10B**) and the obtained Au@CeO_2 NCs were core@shell structures (**Fig. 4C**). Finally, the further increase of the pH towards highly alkaline values (pH 12) resulted in the fast and spontaneous nucleation of isolated CeO_2 NCs away from the surface of the Au seeds (**Fig. S9B**).

Obtained results show how the use of citrate as a complexing agent of $Ce^{3+/4+}$ facilitated control over the oxidation and hydrolysis rates of cerium precursors, reducing their reactivity in water and allowing for a better control of the reaction. In these conditions, the different growth modes of CeO_2 can be adjusted by simply varying the reaction pH. This process determines the tendency of the cerium precursor to (i) homogeneously nucleate (high pH), (ii) hetero-nucleate at the metal surface (mild alkaline), (iii) growth (neutral) or (iv) remain stable in solution (acidic). As stated

previously[37-38], hydroxide ions in solution are highly involved in the formation process of CeO_2 NCs. By decreasing the concentration of hydroxide ions, the oxidation and hydrolysis rates of the complexed cerium ions are further decreased[39-40], which is translated into even slower reaction rates. Under these conditions, the homogeneous nucleation of CeO_2 is prevented while its heterogeneous nucleation onto the Au seeds is promoted. Then, once a small domain of CeO_2 NCs is initially formed on the Au seeds, the subsequent CeO_2 NCs prefers to grow on top of this domain, rather than on the Au surface.[41] This is consistent with the fact that nucleation has higher energy barriers than growth processes, in such a way that nucleation and growth can be separated.[42] At intermediate conditions of pH, multiple nucleation points coexist at the Au NC surface initially forming clover-like (discontinuous) shells that ultimately lead to the core@shell when they grow further.[41] The possibility to adjust the morphology of the hybrid structure and obtain NCs with explicitly different coupling manners between the Au NCs and CeO_2 allows adjusting the properties of the NC. Thus, well-defined Au/CeO_2 heterodimers, where parts of the Au surface are exposed, experience smaller red-shifts than NCs with a uniform CeO_2 coating around the Au cores (**Fig. S10**).

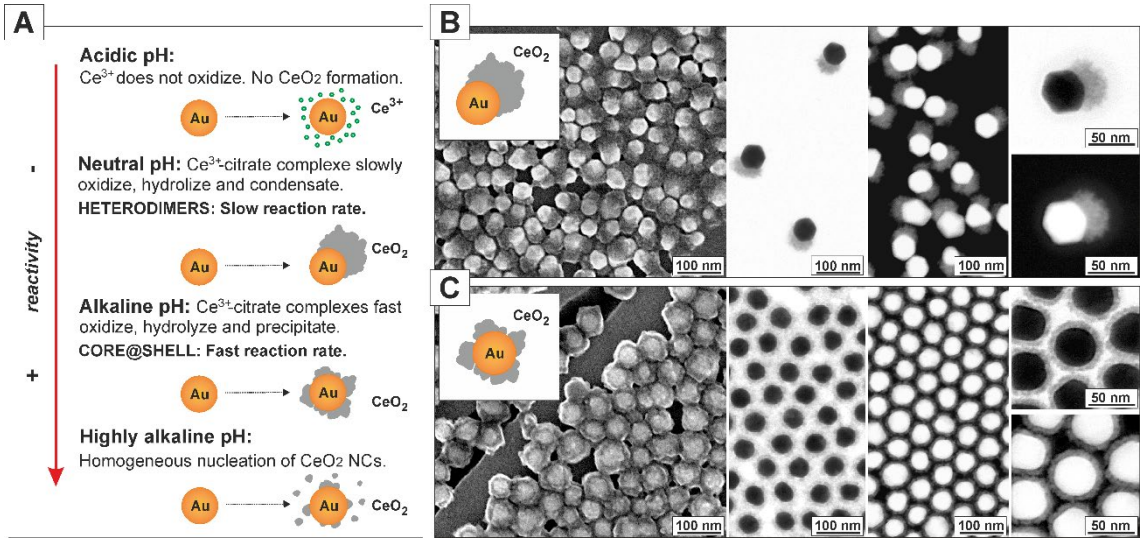

Figure 4. Variation of the architecture of Au/CeO_2 Hybrid NCs. Overall formation mechanism (**A**) and representative SEM, TEM, and HAADF-STEM images (**B, C**) of Au/CeO_2 hybrid NCs obtained by adjusting the pH of the reaction solution. At acidic pH, Ce^{3+} is not oxidized and no CeO_2 deposits onto the Au NCs. At neutral and alkaline pH, Ce^{4+}-citrate is formed. Its reactivity depends on the pH of the solution. At neutral pH, Ce^{4+}-citrate complexes slowly hydrolyze and condensate onto Au NCs leading to heterostructured morphologies (**B**). At alkaline pH, the hydrolysis and precipitation are faster and core@shell structures are promoted (**C**). At highly alkaline pH, the complexing effect of citrate strongly decreases because of the high concentration of competing hydroxides in solution. As a result, the homogeneous nucleation of isolated CeO_2 NCs is not completely prevented.

The versatility of the method allows the precise and deliberate manipulation of the NC architecture by the simultaneous injection of Au^{3+} or Ce^{3+} precursors onto preformed clover-like Au@CeO_2 NCs. As expected, under appropriate conditions, Ce^{3+} oxidizes and deposits onto the existent CeO_2 domains. This process confines the overgrowth of Au onto the accessible ceria-free surface of the hybrid NCs, thereby forcing the formation of highly anisotropic star-like NCs (**Fig. 5**). This change in morphology result into the emergence of a characteristic LSPR band in the region between 600-800 nm (**Fig. 5E**).[44] This intense broadband at the near-infrared region together with the larger interface of anisotropic structures make these NCs promise candidates for NIR-light-driven applications.

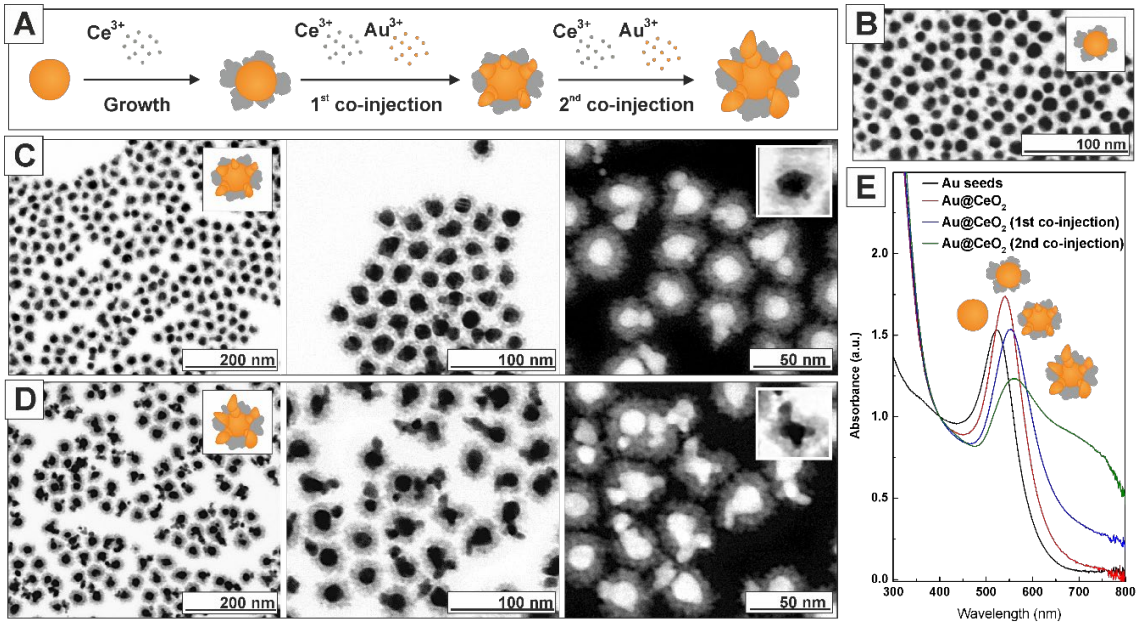

Figure 5. Branched Au/CeO_2 NCs. Precise and deliberate manipulation of the NC architecture by the simultaneous co-injection of Au^{3+} and Ce^{3+} precursors onto preformed Au/CeO_2 NCs (**A**). Representative TEM and HAADF_STEM images of clover-like Au@CeO_2 NCs obtained by the injection of Ce^{3+} precursor onto 15 nm Au NC seeds (**B**), and after 1st (**C**) and 2nd (**D**) co-injection. The large lattice mismatch between CeO_2 and Au favors the epitaxial reduction of Au^{3+} onto the accessible Au domains of the structure and the formation of well-defined branched Au/CeO2 NCs. UV-vis spectra of as-obtained samples (**E**). The broadband in the region between 600-800 nm is assigned to the collective LSPR of the anisotropic Au domain. Additional morphological characterization can be found in Fig. S12.

The presented approach can be extended to other systems. In preliminary experiments, similar citrate-stabilized Ag/CeO_2 NCs were obtained by replacing the Au seeds by Ag seeds (**Fig. 6A**). Similarly, the atom-by-atom CeO_2 deposition occurs and can be controlled also in the presence of surfactants with strong or mild affinity for metal surfaces. Thus, 11-mercaptoundecanoic acid (MUA)- and polyvinylpyrrolidone (PVP)-coated Au seeds were also successfully employed to grow Au@CeO_2 NCs (**Fig. 6B-C**). This point suggests that the method may be adapted to the CeO_2

coating of anisotropic NC seeds, like cubes and rods, obtained by selective attachment of surfactants to certain crystal facets, or the template-induced growth processes.

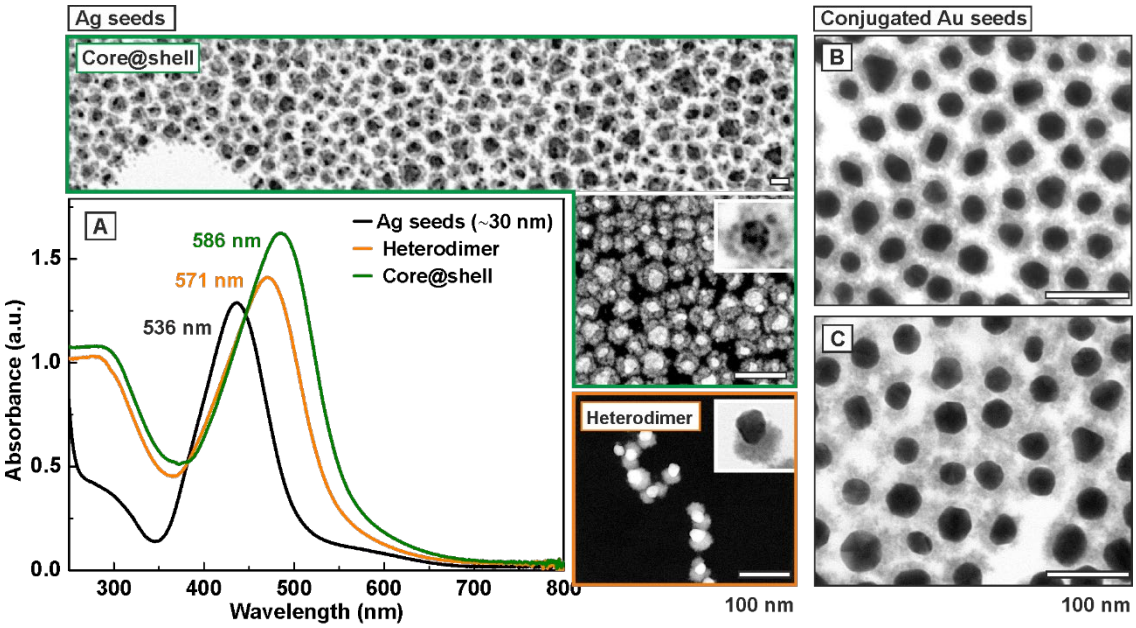

Figure 6. Representative TEM, SEM and HAADF-STEM images and corresponding UV-vis spectra (**A**) of core@shell and heterodimer Ag/CeO_2 NCs obtained using 30 nm Ag seeds. Representative TEM images of Au@CeO_2 NCs obtained using 11-mercaptoundecanoic- (**B**) and 10 KDa PVP- (**C**) stabilized 30 nm Au seeds. Synthesis conditions are detailed in the supporting information.

With the aim of gaining further insight into the impact of the CeO_2 coating on the optical properties of Au NCs, extinction efficiencies of Au spheres of varying diameters and CeO_2 coating thickness have been calculated following the standard Mie theory[45]. **Figure 7** plots individual absorbance spectra, containing both absorption and scattering contributions, calculated for Au spheres of different sizes (5, 10, 15, 30, 40 and 100 nm) coated with a homogeneous CeO_2 shell of different thicknesses (from 0.5 to 20 nm). Results are further summarized by plotting the position of the LSPR band of Au NCs for the different CeO_2 thicknesses (**Fig. 7G**). As can be seen, when the Au cores are coated with the CeO_2 dielectric shell of increasing thickness, the LSPR position shifts gradually towards longer wavelengths and the absorbance increases, saturating at a thickness when the electric field of the plasmon is fully confined inside the dielectric CeO_2 layer. Remarkably, both features (redshift and increase in peak intensity) depend on the size of the Au NC core and can be explained in terms of the size-dependent near-field profiles of the Au NCs.[46] Despite the good correlation between experimental results and Mie calculations, the calculated

LSPR red-shits are systematically larger than those experimentally obtained. These differences are mainly attributed to the "compactness" of the CeO_2 shell. We certainly assume in our calculations that Au NCs are surrounded by a homogeneous CeO_2 coating layer while experimental results suggest that the CeO_2 shell is rather granular (porous) and of low density. This assumption determines the effective dielectric constant of the system, which ultimately affects the extent of the LSPR red-shifts (**Fig. S14**). Although the limitations of the Mie theory, especially for small NC sizes, the good correlation between experimental results and Mie calculations confirms the working hypothesis, that is, the possibility of precisely controlling the strongly enhance local electromagnetic fields near the metal-dielectric interface by adjusting Au core size, and CeO_2 shell thicknesses.

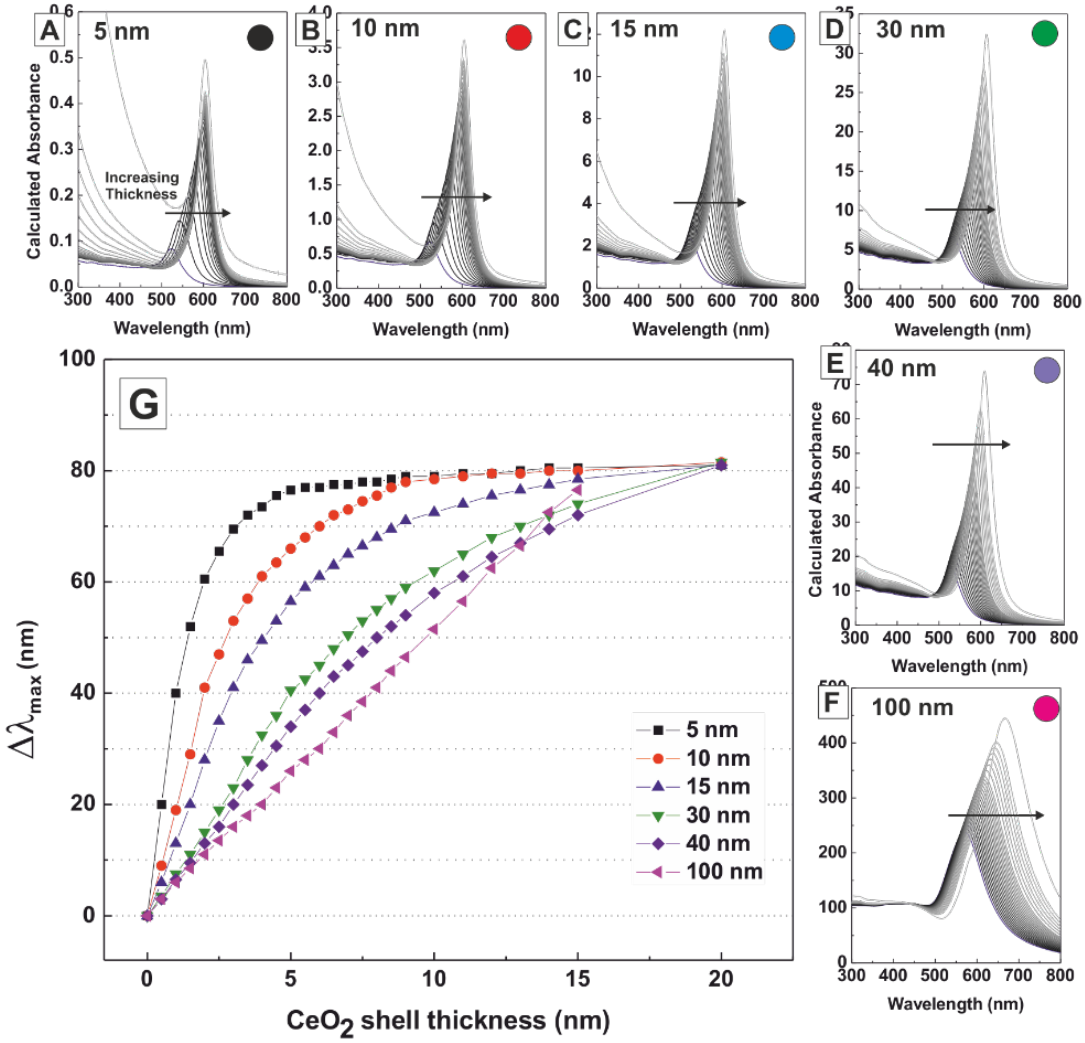

Figure 7. Influence of CeO_2 shell thickness on the optical properties of Au NCs of different sizes. Calculated absorbance spectra of Au spheres before and after their coating with a CeO_2 shell of different thickness (as-labelled). 5 nm (**A**), 10 nm (**B**), 15 nm (**C**), 30 nm (**D**), 40 nm (**E**), 100 nm (**F**). Dependence of the surface plasmon resonance peaks positions for Au NCs of varying sizes (**G**). Calculations were performed considering colloidal solutions of NCs ($3x10^{12}$ NCs/mL) coated by a CeO_2 shell of refractive index 2.2 (20 °C) and dispersed in water (RI = 1.333, 20 °C).[47] For citrate-

stabilized Au NCs, a shell thickness of 0.7 nm and RI=1.3735 was used (SI, section 15). Results reveal the higher sensitivity of the smaller NCs in comparison with the larger sizes for a determined CeO_2 shell thickness. Similar calculations were performed to study the influence of the shell coating on the LSPR peak of Au and Ag NCs of different sizes.[31, 46]

CONCLUSIONS

To summarize, we have developed a novel and simple seeded-growth aqueous approach for the production of well-defined colloidal-stable citrate-stabilized Au/CeO_2 hybrid nanocrystals (NCs) with unprecedented control of their architectural and morphological characteristics. The synthetic strategy, based on the identification of the experimental conditions under which the heterogeneous nucleation and growth processes of CeO_2 onto pre-synthetized Au NCs is controlled, relies on the use of SC which plays multiple key roles as a reducer, pH buffer, complexing, directing and stabilizing agent. The robustness and versatility of the synthetic reaction allows for the fine adjustment of each individual domain in the structure, particularly, the size of the Au core (from 5 nm to 100 nm), the thickness of the CeO_2 shell (from 5 nm to 20 nm) and the growth mode of CeO_2 onto Au (core@shell, clover-like, star-like or heterodimer). Also, the approach allows for studying the impact of fine variations of hybrid NCs on the underlying optical response.

Additionally, the level of morphological control obtained, as well as the ease by which such well-defined nanostructures are produced, opens new opportunities for understanding the nanoscale mechanisms and systematically investigate the interactions between individual components allowing designing new catalysts and optical devices. Remarkably, since no organic solvents are used and no toxic waste is formed during the reaction, the proposed synthesis method can be defined as a sustainable, viable and low-cost strategy to fabricate noble metal/metal oxide NCs. We believe that the results and understanding acquired in this study will contribute to the development of a new generation of highly multifunctional complex hybrid NCs for a wide variety of applications.

SUPPORTING INFORMATION

Details of experimental protocols and conditions studied together with extended NCs characterization are available free of charge via the internet at http://pubs.acs.org.

ACKNOWLEDGMENTS

We acknowledge financial support from the Spanish MINECO (MAT2015-70725-R, ENE2017-85087-C3), MICINN (RTI2018-099965-B-I00) and from the Catalan Agència de Gestió d'Ajuts Universitaris i de Recerca (AGAUR) (2017-SGR-1431, 2017-SGR-327). Financial support from the HISENTS (685817) Project financed by the European Community under H20202 Capacities Programme is gratefully acknowledged. N.G.B. acknowledges financial support by MINECO through the Ramon y Cajal program (RYC-2012- 10991). ICN2 is supported by the Severo Ochoa program from Spanish MINECO (Grant No. SEV-2017-0706) and is funded by the CERCA Programme / Generalitat de Catalunya. Part of the present work has been performed in the framework of the Universitat Autònoma de Barcelona Degree and Ph.D. program.

REFERENCES

1. Bastús, N. G.; Gonzalez, E.; Esteve, J.; Piella, J.; Patarroyo, J.; Merkoçi, F.; Puntes, V., Exploring New Synthetic Strategies for the Production of Advanced Complex Inorganic Nanocrystals. *Z. Phys. Chem.* **2015,** *229* (1-2), 65-83.

2. Cozzoli, P. D.; Pellegrino, T.; Manna, L., Synthesis, properties and perspectives of hybrid nanocrystal structures. *Chem. Soc. Rev.* **2006,** *35* (11), 1195-1208.

3. Costi, R.; Saunders, A. E.; Banin, U., Colloidal Hybrid Nanostructures: A New Type of Functional Materials. *Angewandte Chemie International Edition* **2009,** *49* (29), 4878-4897.

4. Zhao, Q.; Ji, M.; Qian, H.; Dai, B.; Weng, L.; Gui, J.; Zhang, J.; Ouyang, M.; Zhu, H., Controlling Structural Symmetry of a Hybrid Nanostructure and its Effect on Efficient Photocatalytic Hydrogen Evolution. *Adv. Mater.* **2014,** *26* (9), 1387-1392.

5. Carrettin, S.; Concepcion, P.; Corma, A.; Nieto, J. M. L.; Puntes, V. F., Nanocrystalline CeO2 increases the activity of an for CO oxidation by two orders of magnitude. *Angewandte Chemie-International Edition* **2004,** *43* (19), 2538-2540.

6. Divins, N. J.; Angurell, I.; Escudero, C.; Pérez-Dieste, V.; Llorca, J., Influence of the support on surface rearrangements of bimetallic nanoparticles in real catalysts. *Science* **2014,** *346* (6209), 620-623.

7. Lattuada, M.; Hatton, T. A., Synthesis, properties and applications of Janus nanoparticles. *Nano Today* **2011,** *6* (3), 286-308.

8. Seh, Z. W.; Liu, S.; Zhang, S.-Y.; Bharathi, M. S.; Ramanarayan, H.; Low, M.; Shah, K. W.; Zhang, Y.-W.; Han, M.-Y., Anisotropic Growth of Titania onto Various Gold Nanostructures: Synthesis, Theoretical Understanding, and Optimization for Catalysis. *Angewandte Chemie International Edition* **2011,** *50* (43), 10140-10143.

9. Cargnello, M.; Doan-Nguyen, V. V. T.; Gordon, T. R.; Diaz, R. E.; Stach, E. A.; Gorte, R. J.; Fornasiero, P.; Murray, C. B., Control of Metal Nanocrystal Size Reveals Metal-Support Interface Role for Ceria Catalysts. *Science* **2013,** *341* (6147), 771-773.

10. Rai, P.; Majhi, S. M.; Yu, Y.-T.; Lee, J.-H., Noble metal@metal oxide semiconductor core@shell nano-architectures as a new platform for gas sensor applications. *RSC Adv.* **2015,** *5* (93), 76229-76248.

11. Li, J.-F.; Zhang, Y.-J.; Ding, S.-Y.; Panneerselvam, R.; Tian, Z.-Q., Core–Shell Nanoparticle-Enhanced Raman Spectroscopy. *Chemical Reviews* **2017,** *117* (7), 5002-5069.

12. Jiang, R.; Li, B.; Fang, C.; Wang, J., Metal/Semiconductor Hybrid Nanostructures for Plasmon-Enhanced Applications. *Adv. Mater.* **2014,** *26* (31), 5274-5309.

13. Li, G.; Tang, Z., Noble metal nanoparticle@metal oxide core/yolk–shell nanostructures as catalysts: recent progress and perspective. *Nanoscale* **2014,** *6* (8), 3995-4011.

14. Montini, T.; Melchionna, M.; Monai, M.; Fornasiero, P., Fundamentals and Catalytic Applications of CeO2-Based Materials. *Chem. Rev.* **2016,** *116* (10), 5987-6041.

15. Centeno, M. A.; Ramírez Reina, T.; Ivanova, S.; Laguna, O. H.; Odriozola, J. A., Au/CeO2 Catalysts: Structure and CO Oxidation Activity. *Catalysts* **2016,** *6* (10), 158.

16. Huang, P. X.; Wu, F.; Zhu, B. L.; Gao, X. P.; Zhu, H. Y.; Yan, T. Y.; Huang, W. P.; Wu, S. H.; Song, D. Y., CeO2 Nanorods and Gold Nanocrystals Supported on CeO2 Nanorods as Catalyst. *J. Phys. Chem. B* **2005,** *109* (41), 19169-19174.

17. Djuricic, B.; Pickering, S., Nanostructured cerium oxide: preparation and properties of weakly-agglomerated powders. *J. Eur. Ceram. Soc.* **1999,** *19* (11), 1925-1934.

18. Han, M.; Wang, X.; Shen, Y.; Tang, C.; Li, G.; Smith, R. L., Preparation of Highly Active, Low Au-Loaded, Au/CeO2 Nanoparticle Catalysts That Promote CO Oxidation at Ambient Temperatures. *J. Phys. Chem. C* **2010,** *114* (2), 793-798.

19. Alivisatos, P.; Barbara, P. F.; Castleman, A. W.; Chang, J.; Dixon, D. A.; Klein, M. L.; McLendon, G. L.; Miller, J. S.; Ratner, M. A.; Rossky, P. J.; Stupp, S. I.; Thompson, M. E., From Molecules to Materials: Current Trends and Future Directions. *Adv. Mater.* **1998,** *10* (16), 1297-1336.

20. Mitsudome, T.; Yamamoto, M.; Maeno, Z.; Mizugaki, T.; Jitsukawa, K.; Kaneda, K., One-step Synthesis of Core-Gold/Shell-Ceria Nanomaterial and Its Catalysis for Highly Selective Semihydrogenation of Alkynes. *J. Am. Chem. Soc.* **2015,** *137* (42), 13452-13455.

21. Kayama, T.; Yamazaki, K.; Shinjoh, H., Nanostructured Ceria–Silver Synthesized in a One-Pot Redox Reaction Catalyzes Carbon Oxidation. *J. Am. Chem. Soc.* **2010,** *132* (38), 13154-13155.

22. Mitsudome, T.; Mikami, Y.; Matoba, M.; Mizugaki, T.; Jitsukawa, K.; Kaneda, K., Design of a Silver–Cerium Dioxide Core–Shell Nanocomposite Catalyst for Chemoselective Reduction Reactions. *Angewandte Chemie International Edition* **2012,** *51* (1), 136-139.

23. Mitsudome, T.; Matoba, M.; Mizugaki, T.; Jitsukawa, K.; Kaneda, K., Core–Shell AgNP@CeO_2 Nanocomposite Catalyst for Highly Chemoselective Reductions of Unsaturated Aldehydes. *Chem. - Eur. J.* **2013,** *19* (17), 5255-5258.

24. Ji, X.; Song, X.; Li, J.; Bai, Y.; Yang, W.; Peng, X., Size Control of Gold Nanocrystals in Citrate Reduction: The Third Role of Citrate. *J. Am. Chem. Soc.* **2007,** *129* (45), 13939-13948.

25. Li, B.; Gu, T.; Ming, T.; Wang, J.; Wang, P.; Wang, J.; Yu, J. C., (Gold Core)@(Ceria Shell) Nanostructures for Plasmon-Enhanced Catalytic Reactions under Visible Light. *ACS Nano* **2014,** *8* (8), 8152-8162.

26. Qi, J.; Chen, J.; Li, G.; Li, S.; Gao, Y.; Tang, Z., Facile synthesis of core–shell Au@CeO2 nanocomposites with remarkably enhanced catalytic activity for CO oxidation. *Energy & Environmental Science* **2012,** *5* (10), 8937-8941.

27. Cargnello, M.; Gentilini, C.; Montini, T.; Fonda, E.; Mehraeen, S.; Chi, M. F.; Herrera-Collado, M.; Browning, N. D.; Polizzi, S.; Pasquato, L.; Fornasiero, P., Active and Stable Embedded Au@CeO2 Catalysts for Preferential Oxidation of CO. *Chem. Mater.* **2010,** *22* (14), 4335-4345.

28. Cargnello, M.; Wieder, N. L.; Montini, T.; Gorte, R. J.; Fornasiero, P., Synthesis of dispersible Pd@CeO(2) core-shell nanostructures by self-assembly. *J Am Chem Soc* **2010,** *132* (4), 1402-9.

29. Wang, X.; Liu, D.; Song, S.; Zhang, H., Pt@CeO2 Multicore@Shell Self-Assembled Nanospheres: Clean Synthesis, Structure Optimization, and Catalytic Applications. *J. Am. Chem. Soc.* **2013,** *135* (42), 15864-15872.

30. Zhang, S.; Chen, C.; Cargnello, M.; Fornasiero, P.; Gorte, R. J.; Graham, G. W.; Pan, X., Dynamic structural evolution of supported palladium–ceria core–shell catalysts revealed by in situ electron microscopy. *Nature Communications* **2015,** *6*, 7778.

31. Bastús, N. G.; Comenge, J.; Puntes, V. F., Kinetically Controlled Seeded Growth Synthesis of Citrate-Stabilized Gold Nanoparticles of up to 200 nm: Size Focusing versus Ostwald Ripening. *Langmuir* **2011,** *27* (17), 11098-11105.

32. Bastús, N. G.; Merkoçi, F.; Piella, J.; Puntes, V., Synthesis of Highly Monodisperse Citrate-Stabilized Silver Nanoparticles of up to 200 nm: Kinetic Control and Catalytic Properties. *Chem. Mater.* **2014,** *26* (9), 2836-2846.

33. Bobtelsky, M.; Graus, B., Cerous Citrate Complexes, their Composition, Structure and Behavior. *J. Am. Chem. Soc.* **1955,** *77* (7), 1990-1993.

34. Piella, J.; Bastus, N. G.; Puntes, V., Size-Controlled Synthesis of Sub-10-nanometer Citrate-Stabilized Gold Nanoparticles and Related Optical Properties. *Chem. Mater.* **2016,** *28* (4), 1066-1075.

35. Seh, Z. W.; Liu, S.; Low, M.; Zhang, S.-Y.; Liu, Z.; Mlayah, A.; Han, M.-Y., Janus Au-TiO2 Photocatalysts with Strong Localization of Plasmonic Near-Fields for Efficient Visible-Light Hydrogen Generation. *Advanced Materials* **2012,** *24* (17), 2310-2314.

36. Zhang, Q.; Zhang, T.; Ge, J.; Yin, Y., Permeable Silica Shell through Surface-Protected Etching. *Nano Lett.* **2008,** *8* (9), 2867-2871.

37. Chen, H.-I.; Chang, H.-Y., Synthesis of nanocrystalline cerium oxide particles by the precipitation method. *Ceram. Int.* **2005,** *31* (6), 795-802.

38. Bouchaud, B.; Balmain, J.; Bonnet, G.; Pedraza, F., pH-distribution of cerium species in aqueous systems. *Journal of Rare Earths* **2012,** *30* (6), 559-562.

39. Zhou, X.-D.; Huebner, W.; Anderson, H. U., Room-temperature homogeneous nucleation synthesis and thermal stability of nanometer single crystal CeO 2. *Applied Physics Letters* **2002,** *80* (20), 3814-3816.

40. Chen, P. L.; Chen, I. W., Reactive cerium (IV) oxide powders by the homogeneous precipitation method. *Journal of the American Ceramic Society* **1993,** *76* (6), 1577-1583.

41. Bastús, N. G.; Piella, J.; Perez, S.; Patarroyo, J.; Genç, A.; Arbiol, J.; Puntes, V., Robust one-pot synthesis of citrate-stabilized Au@CeO2 hybrid nanocrystals with different thickness and dimensionality. *Applied Materials Today* **2019,** *15*, 445-452.

42. Peng, X.; Wickham, J.; Alivisatos, A. P., Kinetics of II-VI and III-V Colloidal Semiconductor Nanocrystal Growth: "Focusing" of Size Distributions. *J. Am. Chem. Soc.* **1998,** *120* (21), 5343-5344.

43. Hirano, M.; Kato, E., Hydrothermal Synthesis of Nanocrystalline Cerium(IV) Oxide Powders. *Journal of the American Ceramic Society* **1999,** *82* (3), 786-788.

44. Barbosa, S.; Agrawal, A.; Rodriguez-Lorenzo, L.; Pastoriza-Santos, I.; Alvarez-Puebla, R. A.; Kornowski, A.; Weller, H.; Liz-Marzan, L. M., Tuning size and sensing properties in colloidal gold nanostars. *Langmuir* **2010,** *26* (18), 14943-50.

45. Juluri, B. K.; Huang, J.; Jensen, L. *Extinction, Scattering and Absorption efficiencies of single and multilayer nanoparticles*, 2012.

46. Bastus, N. G.; Piella, J.; Puntes, V., Quantifying the Sensitivity of Multipolar (Dipolar, Quadrupolar, and Octapolar) Surface Plasmon Resonances in Silver Nanoparticles: The Effect of Size, Composition, and Surface Coating. *Langmuir* **2016,** *32* (1), 290-300.

47. Piella, J.; Bastús, N. G.; Puntes, V., Modeling the Optical Responses of Noble Metal Nanoparticles Subjected to Physicochemical Transformations in Physiological Environments: Aggregation, Dissolution and Oxidation. *Z. Phys. Chem.* **2017,** *231* (1), 33-50.